Electronic Supplementary Material (ESI) for Journal of Materials Chemistry A.

Electronic Supplementary Information

Chainmail Catalyst of Ultrathin P-doped Carbon Shell Encapsulated Nickel Phosphides on Graphene towards Robust and Efficient Hydrogen Generation

Mao Miao, [a] *Ruizuo Hou,* [a] *Zhun Liang,* [b] *Ruijuan Qi,* [c] *Ya Yan,* [d] *Ting He,* [a] *Kai Qi,* [a] *Hongfang Liu,* [a] *Guang Feng,* [b] *Bao Yu Xia* [a] [*]

[a] *Key Laboratory of Material Chemistry for Energy Conversion and Storage (Ministry of Education), Hubei Key Laboratory of Material Chemistry and Service Failure, School of Chemistry and Chemical Engineering, Wuhan National Laboratory for Optoelectronics, Huazhong University of Science and Technology (HUST), 1037 Luoyu Road, Wuhan 430074, P. R. China*

[b] *State Key Laboratory of Coal Combustion, School of Energy and Power Engineering, Huazhong University of Science and Technology, 1037 Luoyu Road, Wuhan 430074, P. R. China.*

[c] *School of Information Science and Technology, East China Normal University, 500 Dongchuan Road, Shanghai 200241, P. R. China*

[d] *School of Materials Science and Engineering, University of Shanghai for Science and Technology, 516 Jungong Road, Shanghai 200093, P. R. China*

**Corresponding author: byxia@hust.edu.cn (B. Y. Xia)*

1. Preparation of Materials:

All chemicals were used as received. $NiCl_2\cdot6H_2O$, $NaH_2PO_2\cdot H2O$, *N, N*-Dimethylformamide (DMF), KOH and concentrated H_2SO_4 were purchased from *Sinopharm Chemical Reagent Co., Ltd*. DI water was obtained at 18.2 Ω. In a typical experiment, $NiCl_2\cdot6H_2O$ (2mmol, 0.475g), $NaH_2PO_2\cdot H_2O$ (1 mmol, 0.106 g) and GO solution (12 mg mL^{-1}, 3.5 mL) were homogeneously dispersed in a mixture solvent of 10 mL DI water and 10 mL DMF. After vigorously stirring and ultrasonication for 30 min, respectively, the mixture was poured into Teflon-lined stainless steel autoclave (50 mL), then the sealed autoclave was maintained at 160℃ for 16h. When the reaction finished, the autoclave could naturally cool down to room temperature. The black precipitates were collected by centrifuge, washed by DI water and absolute ethanol each for three time to remove the unreacted reactants and soluble impurities. Finally, the as-prepared sample was freeze dried overnight. The as-prepared precursor in quartz boat was placed in an evacuated quartz tube furnace and annealed under reducing atmosphere (the flow ratio of Ar and H_2 was 45:5) at 500 ℃ for 4h with a heating rate of 5°C/min, then the quartz tube furnace could naturally cool down to room temperature. The contrast material Ni_2P MS was synthesized without adding GO solution. Ni_2P/C was fabricated by replacing GO solution with XC-72R.

2. Characterization.

X-ray diffraction (XRD) patterns was conducted on a PANalytical B.V. x'pert3 powder X-ray diffractometer with Cu Kα radiation (λ=1.5405Å) at 30 kV and 20 mA from 10° to 80° with a scanning increment of 0.02°. Scanning electron microscopy (SEM) and energy-dispersive X-ray analysis (EDX) were conducted with a field-emission scanning electron microscope (FESEM, Nova NanoSEM 450) at an accelerating voltage of 10 kV. Transmission electron microscopy (TEM) and high-resolution transmission electron microscopy (HR-TEM) images were obtained with a Tecnai G2 20 scope at an acceleration voltage of 200 kV. High-angle annular dark field (HAADF) imaging and energy-dispersive spectrometry (EDS) elemental mapping analysis were performed in scanning transmission electron microscopy (STEM) mode on an aberration-corrected FEI Titan G2 60-300 field emission transmission electron microscope, operated at 300 kV (α_{max} = ~100 mrad). Raman spectra were recorded on a LabRAM HR800 instrument with a Nd: YAG laser source of 532 nm in a macroscopic configuration. All XPS spectra were collected by a monochromatic Al-Kα X-ray source (hv = 1486.6 eV, Kratos, AXIS-ULTRA DLD-600W). Inductively coupled plasma mass spectrometer (ICP-MS) were obtained from PerkinElmer ELAN DRC-e instrument.

3. Electrochemical measurement.

All electrochemical measurements were performed using an AutoLab (PGSTAT302N) electrochemical workstation with a typical three electrode system in electrolyte at 25°C. Ag/AgCl (saturated) and Hg/HgO was used as reference electrode in acid (0.5 M H_2SO_4, pH=0) and alkaline (1.0 M KOH, pH=13.6) electrolyte, respectively. Graphite rod was used as counter electrode. A glassy carbon electrode (GCE, diameter of 0.5 cm, 0.196 cm^{-2} in area) covered with catalysts was used as working electrode which was prepared as follows: 5 mg of the as-prepared catalyst was dispersed in 500 μL of ethanol containing 0.25% Nafion, then assisted with sonication treatment for at least 30 min to get a homogenous ink, 10 μL ink was carefully dropped onto the GCE via micropipettor, and the electrode was allowed to dry at room temperature. The mass loading of the electrode was calculated to be 0.51 mg cm^{-2}. Before test, the electrolyte was purged with N_2 gas.

Linear sweep voltammograms (LSVs) in acid (0.5 M H_2SO_4) and in alkaline (1.0 M KOH) electrolyte were recorded from 0V to -0.5 V (vs. RHE) at a scan rate of 5 mV s^{-1}. All potentials were referenced to a reversible hydrogen electrode (RHE) with 90% iR correction: $E_{vs.RHE} = E_{vs.Ag/AgCl} + 0.197 + 0.059pH - iR$, $E_{vs.RHE} = E_{vs.Hg/HgO} + 0.098 + 0.059pH – iR$, where the R was referred to the average ohmic resistance obtained from EIS measurement. Electrochemical Impedance Spectroscopy (EIS) were measured at -0.15 V (vs. RHE) with the AC voltage amplitude of 5 mV and the frequency range from 10^5 Hz to 0.1 Hz. Cyclic voltammograms (CVs) were recorded from 0.097 V to 0.197 V (*vs.* RHE, -0.1 V~ 0 V vs Ag/AgCl) at different scan rates. These CV curves within non-faradaic region centered at the open circuit potential (OCP) with a potential window of 0.1 V are recorded to estimate the double layer capacitance (C_{dl}) of the catalysts. The long term stability of the catalysts characterized by continuous cyclic voltammograms was recorded from 0V to -0.5 V (vs. RHE) at 100 mV s^{-1}. The extended durability was also characterized by chronopotentiometric test with a constant current density at -10 mA cm^{-2} for 25 h.

The effective electrochemical active surface area (ECSA) of the catalysts is calculated according to the equation ECSAs = C_{dl}/C_s, where Cs is the specific capacitance of the material or the capacitance of an atomically smooth planar surface of the material per unit area under identical electrolyte conditions, here, we use general specific capacitances of Cs = 0.04 mF cm^{-2} in 1.0 M KOH according to recent reports.[1-3] The turnover frequency (TOF) was calculated according to the equation: TOF=$\frac{jS}{2nF}$. Where j is the current density at an overpotential of -150 mV, S is the geometric surface area of GC electrode (0.196 cm^2), 2 stands for a two electron reaction process in HER, F is Faraday constant (96,485.3 mol/C), n is the number of moles of metal atoms deposited onto the GC electrodes that calculated from mass loading (0.51 mg cm^{-2}, the molar mass of Ni_2P: 148.35) and ICP-MS results (every metal atom is regard as being able to catalyze the reaction). [2,4]

The kinetic current density for HER was fitted with simplified Butler–Volmer equation:

$$j_k = j_0(e^{\frac{\alpha F}{RT}\eta} - e^{-(\frac{1-\alpha}{RT})\eta})$$

Where j_0 is the exchange current density obtained from the intersection between extrapolated Tafel plot and X axis. α is the transfer coefficient (set as 0.5) with respect to the symmetry of the HER/HOR, which set as 0.5, in accordance with literature. F, R, and T are Faraday's constant (96485 C mol^{-1}), the universal gas constant (8.314 J mol^{-1} K^{-1}), and the temperature in Kelvin (around 298 K), respectively. η is the applied overpotential (in V).

Note: the calculation of interfacial angle:

According to literature, the interfacial angle of hexagonal crystal system (hcp) can be calculated as:[5]

$$\cos\Phi = \frac{h_1h_2 + k_1k_2 + \frac{1}{2}(h_1 1k_2 + h_2k_1) + \frac{3a^2}{4c^2}l_1l_2}{\sqrt{(h_1{}^2 + k_1{}^2 + h_1k_1 + \frac{3a^2}{4c^2}l_1{}^2)(h_2{}^2 + k_2{}^2 + h_2k_2 + \frac{3a^2}{4c^2}l_2{}^2)}}$$

Where (h_1, k_1, l_1) = (1, 1, 1), (h_2, k_2, l_2) = (2, 1, 0), a=b=5.86, and c=3.37.

4. DFT calculation

The density functional theory (DFT) calculations were performed using the plane-wave technique implemented in the Vienna ab initio Simulation package (VASP).[6] The electron-ion interactions were described by the projector-augmented plane wave (PAW) pseudopotentials.[7,8] The revised Perdew-Burke-Ernzerhof (RPBE) functional was used for the exchange and correlation term. The dispersion correction of the D3 correction method by Grimme et al. was also included.[9,10] A plane-wave cutoff energy was set to 470 eV and the spin-polarization was adopted for all computations. The convergences of energy and forces were taken as 10^{-4} eV and 0.05 eV/Å, respectively. All the atoms are free to relax during the structure optimization. The 7×7×13 Monkhorst-Pack grid k-points were employed for the structure optimization of unit cell of Ni_2P, while the gamma k-points was adopted for others since the system is quite large.

The free energy of H adsorption (ΔG_{H*}, H* means an adsorbed H atom) is computed to evaluate the HER activity of each system and can be obtained by

$$\Delta G_{H*} = \Delta E_{H*} + \Delta E_{ZPE} - T\Delta S \qquad (1)$$

where the ΔE_{H*}, ΔE_{ZPE}, and ΔS are the binding energy, zero-point energy (ZPE) change, and entropy change of adsorption H, respectively.[11,12] The value of ΔE_{ZPE}-$T\Delta S$ term is near 0.24 eV and thus ΔG_{H*} is calculated by ΔE_{H*} + 0.24 eV in this work.[13]

A 1×1×2 supercell of Ni_2P encapsulated in a carbon shell (labeled as Ni_2P@C) was built first. For the structure model of hexagonal Ni_2P structure, the calculated cell parameters are a =b = 5.862 Å, and c = 3.372 Å, which is in good agreement with the experimental value (a = b = 5.86 Å and c = 3.37 Å). The model of carbon shell is constructed as C180 (a = b = 2.46 Å, c= 2.8Å) comprising 180 C atoms. The differential charge density was computed to determine the possible adsorption sites. The differential charge density of Ni1-4-8 region is similar with Ni2-3-2, which indicates that the HER activity of these four sites (sites 2, 3, 4 and 8) would be similar. As a result, the sites 4 and 6, which could show different HER activity, are chosen to be the possible H adsorption and P doped sites, respectively. Moreover, since there is a significant charge transfer from Ni1 to site 4 compared with site 6, the atomic charge of site 4 should be smaller than site 6, which is proved by the Bader analysis and listed in Table S4 (-0.08 for site 4 and -0.01 for site 6).

According to the atomic charge of Ni_2P@C H′ and Ni_2P@C H″ (H′ and H″ represent H* adsorbed on site 4 and site 6, respectively), the C site with adsorbed H would transfer their electrons to neighboring C atoms after the H adsorption, which leads to the positively charged H (0.09 for Ni_2P@C H′, 0.04 for Ni_2P@C H″) and the increased atomic charge of the adsorbing C. As a result, the atomic charge of site 4 with H adsorption is -0.01e, while the charge of site 6 with H adsorption is 0.06e. Herein, the charge interaction between site 4 and H′ (-0.01e for site 4 and 0.09e for H′) is stronger than that between site 6 and H″ (0.06e for site 6 and 0.04e for H″), which causes smaller ΔG_{H*} of Ni_2P@C H′ than Ni_2P@C H″. The similar mechanism also takes place in Ni_2P@PC. In general, the doped P atom could transfer its electrons to its adjacent atoms, including the adsorbed H. The charge of H″ in Ni_2P@PC (-0.40e) is negative, while the charge of H′ in Ni_2P@PC (0.08e) is positive. Therefore, the interaction between H′ and site 4 is stronger than between H″ and site 6 for Ni_2P@PC which is consistent with the order of corresponding ΔG_{H*} value.

Figures and Tables

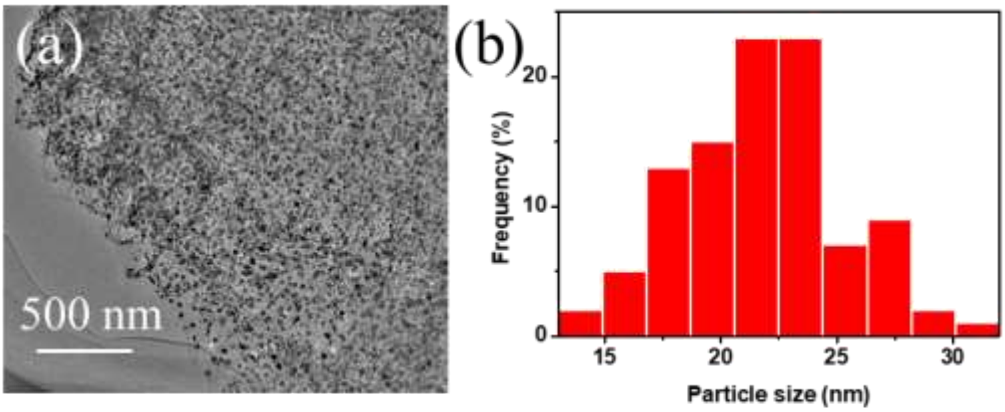

Figure S1. The (a) TEM image of Ni_2P@rGO and (b) The statistical particle size distribution of 100 particles in (a).

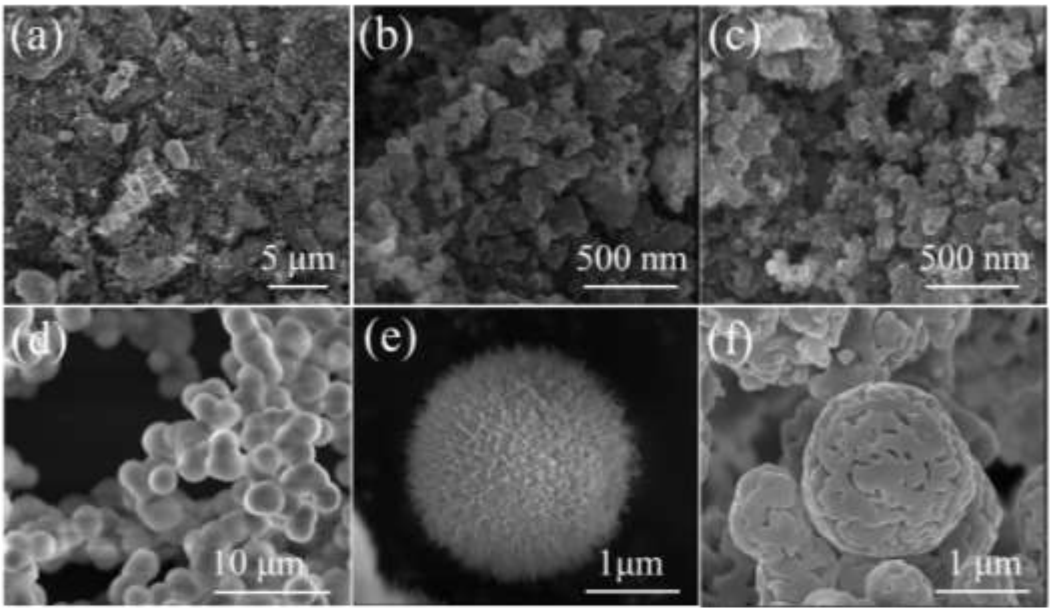

Figure S2. (a-c) SEM images of Ni-P/C: (a, b) precursor, (c) annealed Ni_2P/C. (d-f) Ni-P microspheres: (d, e) precursor, (f) annealed Ni_2P MS.

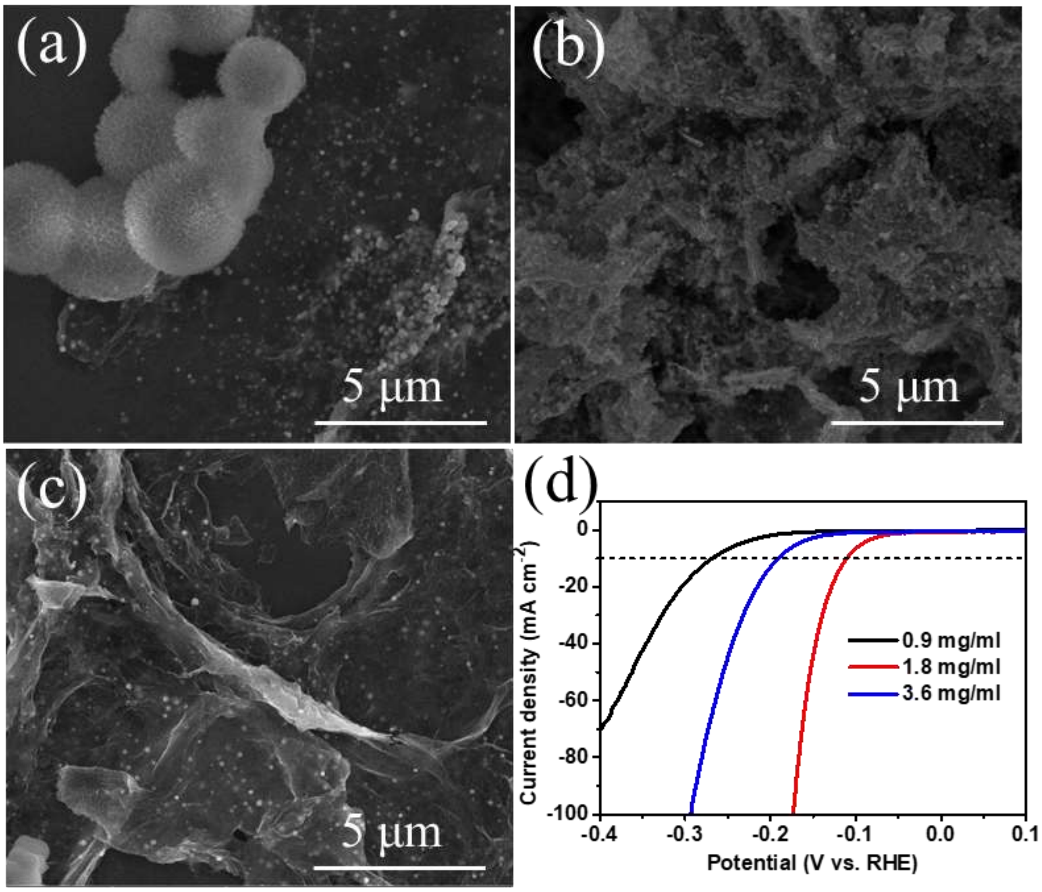

Figure S3. SEM images of precursors with different GO concentration. (a) 0.9 mg mL^{-1}; (b) 1.8 mg mL^{-1}; (c) 3.6 mg mL^{-1}. (d) The corresponding HER performance of various materials in 0.5 M H_2SO_4 (scan rate: 5mV/s).

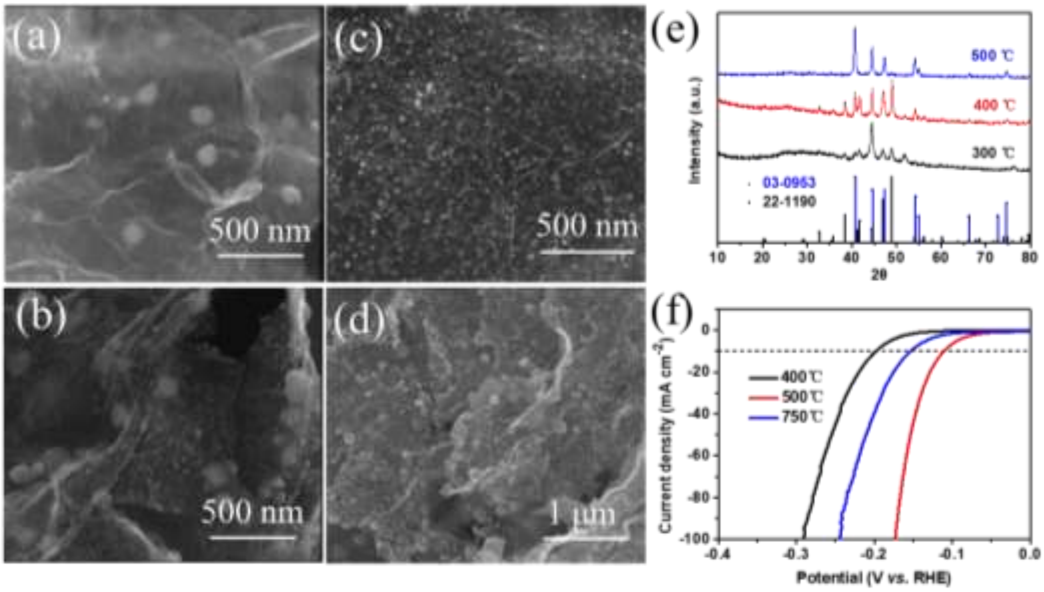

Figure S4. The precursor annealed under different temperature. (a) 300 ℃, (b) 400 ℃, (c) 500 ℃, (d) 750 ℃. (e) The powder XRD pattern of the as-prepared materials. (f) The corresponding HER performance of various materials in 0.5 M H_2SO_4 (scan rate: 5mV/s).

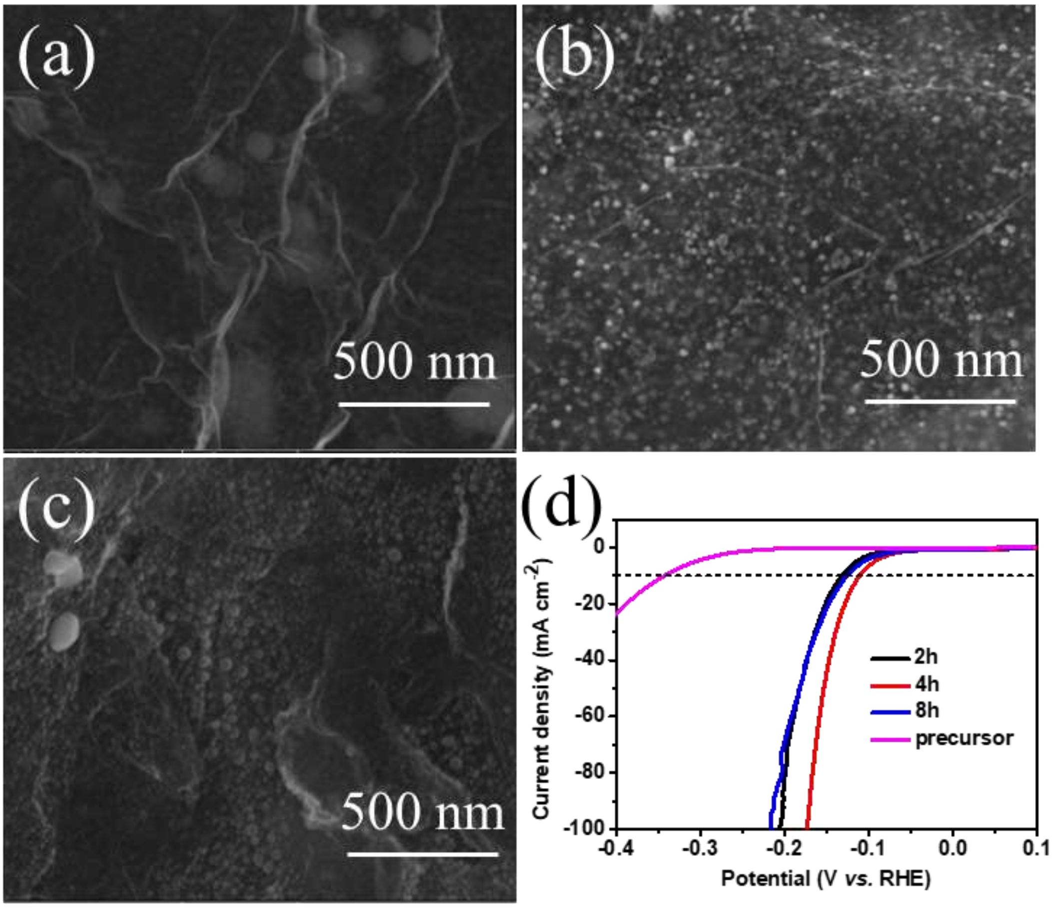

Figure S5. The precursor annealed under 500 ℃ for different duration. (a) 2h, (b) 4h, (c) 8h. (d) The corresponding HER performance of various materials in 0.5 M H_2SO_4 (scan rate: 5mV/s).

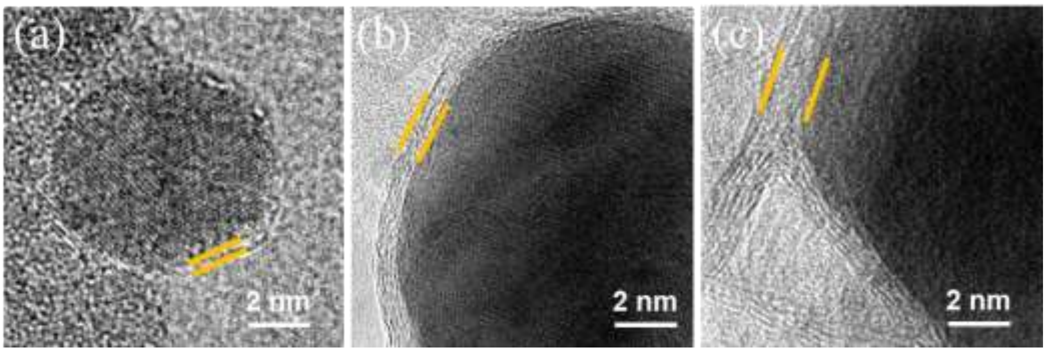

Figure S6. The HR-TEM images of materials annealed under 500 ℃ for different duration. (a) 2h, (b) 4h, (c) 8h. As we can see from these figures that with the increase of annealing time, the carbon shell outside the Ni_2P core is getting thicker, with 4h be the moderate 2~5 layers, which show optimum performance toward HER, as shown in Figure S4d, in consistent with literature.

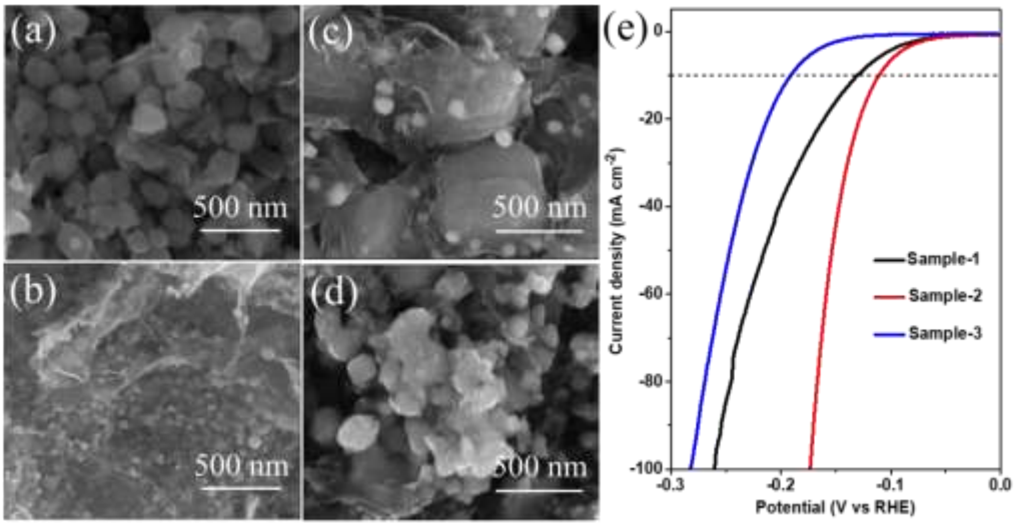

Figure S7. The comparison of different products with different $NiCl_2•6H_2O$ content involved. Sample-1: half $NiCl_2•6H_2O$ and Sample-3: double $NaH_2PO_2•H_2O$. SEM images of (a) precursor and (b) annealed Sample-1. SEM images of (c) precursor and (d) annealed Sample-3. (e) The corresponding HER performance of various materials in 0.5 M H_2SO_4 (scan rate: 5mV/s).

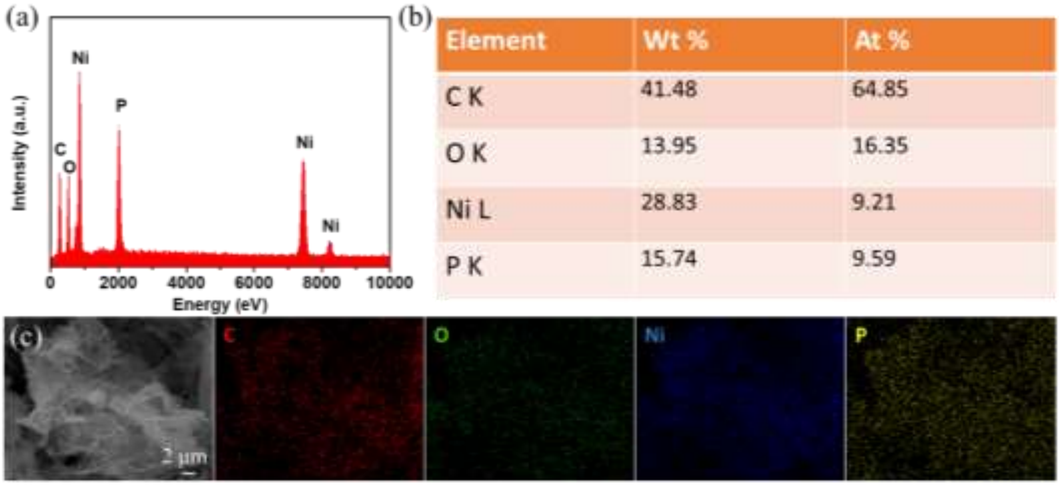

Element	Wt %	At %
C K	41.48	64.85
O K	13.95	16.35
Ni L	28.83	9.21
P K	15.74	9.59

Figure S8. (a) SEM and (b) EDX elemental contents of Ni_2P@PCG, (c) the elemental mapping images of C, O, Ni and P.

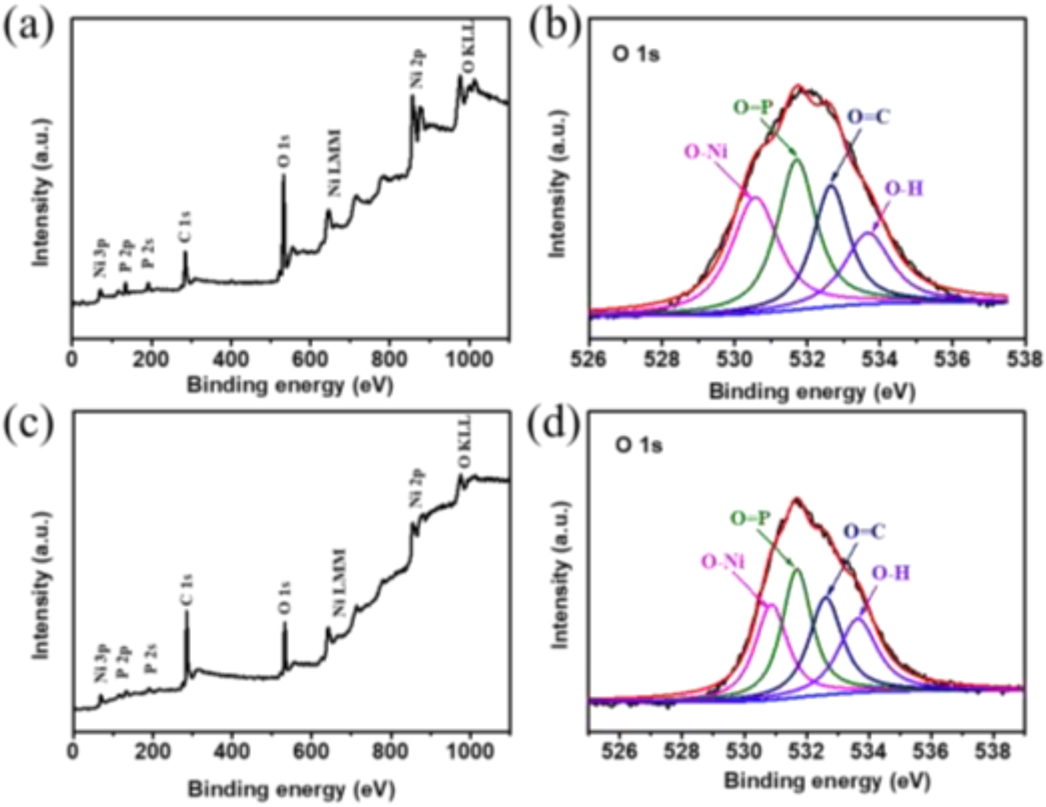

Figure S9. XPS survey spectra of precursor and Ni_2P@PCG (a) Full spectrum and (b) High-resolution XPS spectra of O 1s of precursor. (c) Full spectrum and (d) High-resolution XPS spectra of O 1s of Ni_2P@PCG.

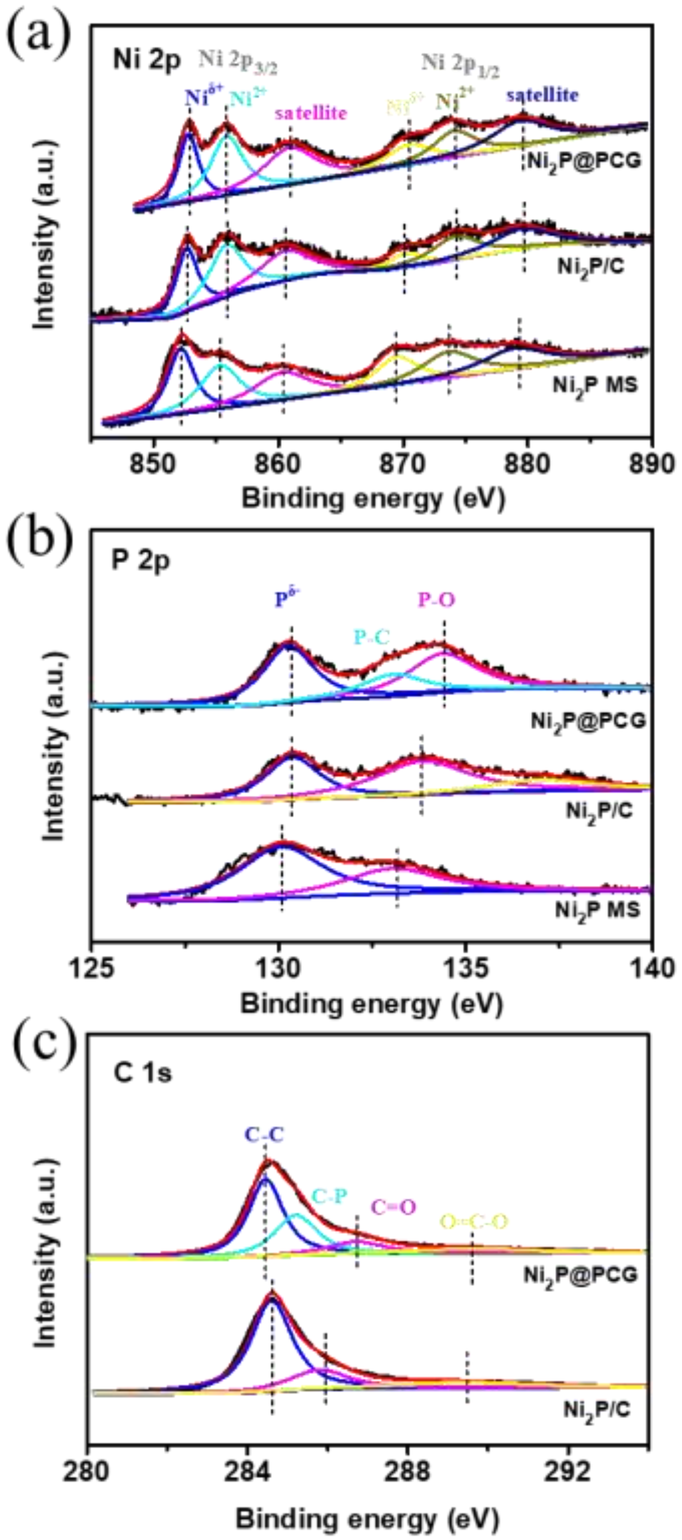

Figure S10. Comparison of XPS survey spectra of Ni$_2$P@PCG, Ni$_2$P/C and Ni$_2$P MS. (a) Ni 2p, (b) P 2p, (c) C 1s.

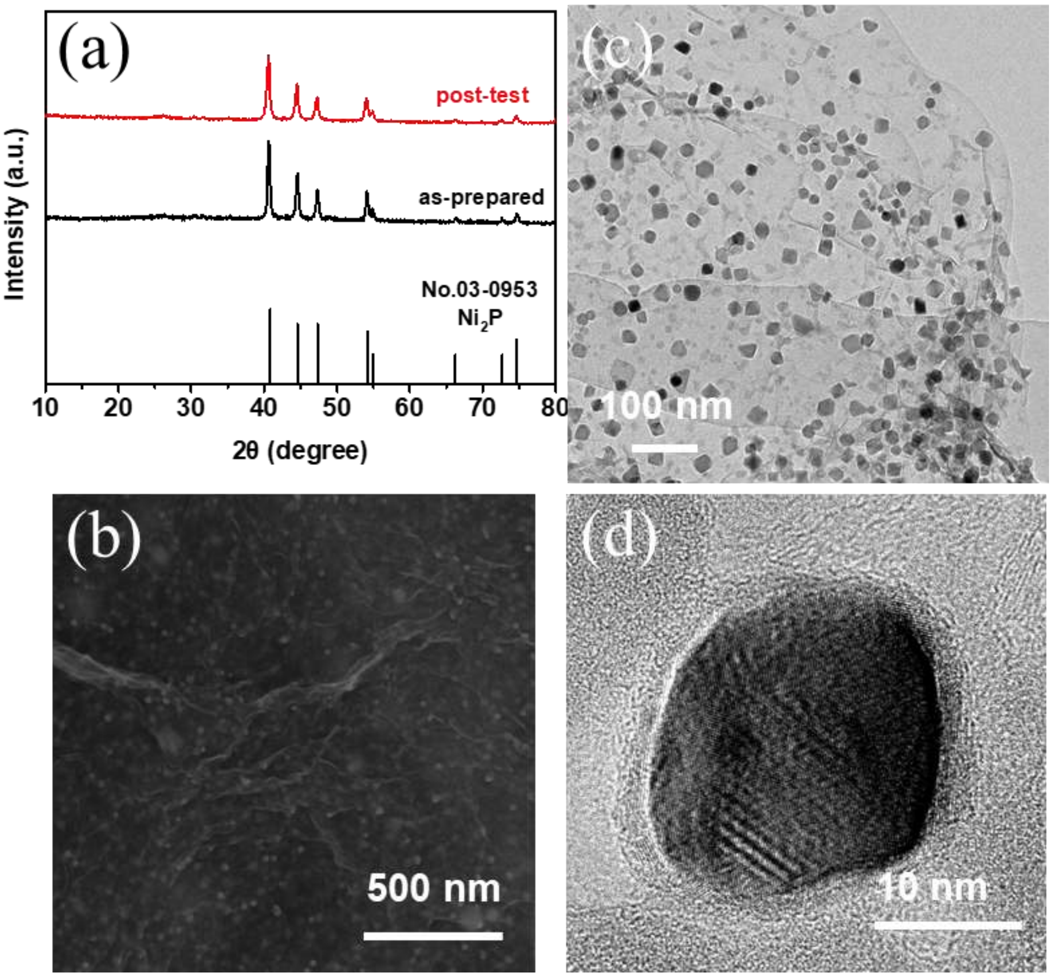

Figure S11. The characterization of post-test material. (a) XRD pattern. (b) SEM and (c) TEM images. (d) HR-TEM image.

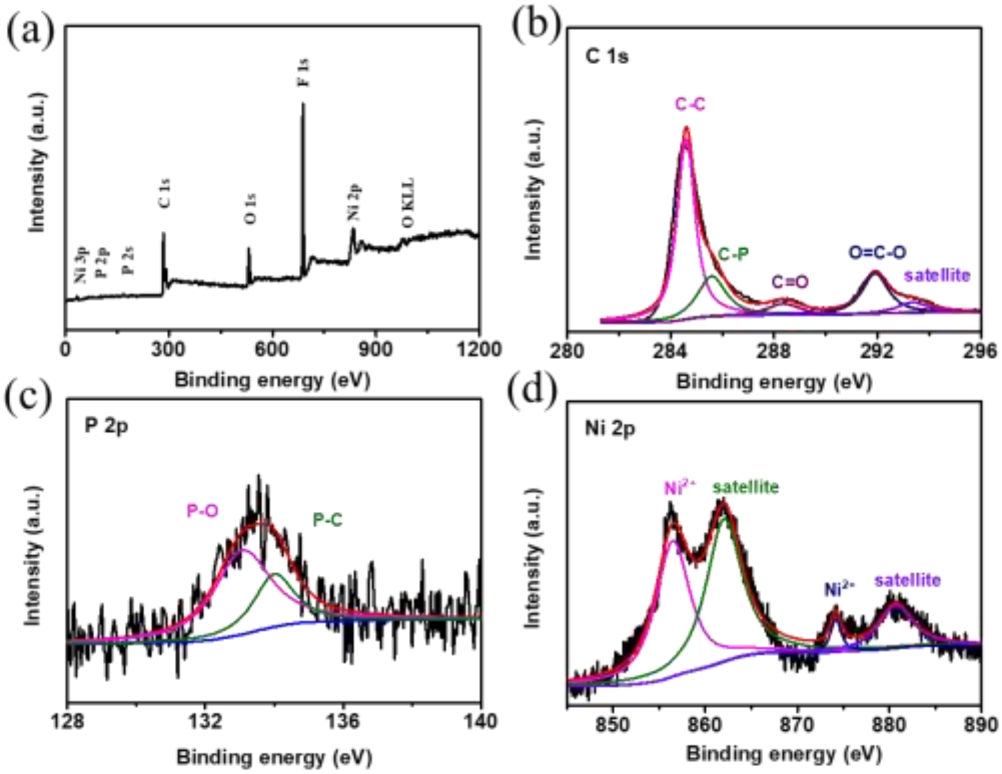

Figure S12. The XPS survey of post-test material. (a) Full spectrum, and High-resolution spectra of (b) C 1s, (c) P 2p and (d) Ni 2p.

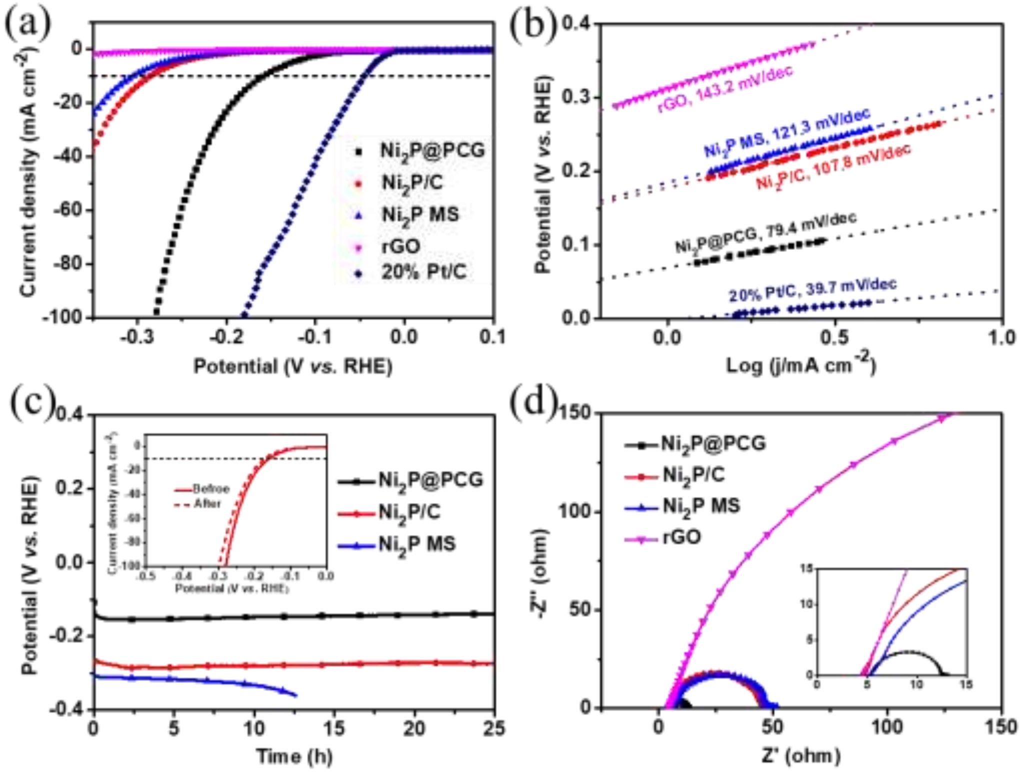

Figure S13. HER performance in 1.0 M KOH. (a) LSV curves (b) Tafel plots, (c) stability test at 10 mA cm^{-2} for 25h, the inset show LSV curves of Ni$_2$P@PCG before and after 5000 cycles, (d) EIS Nyquist plots at -0.3 V (*vs.* RHE).

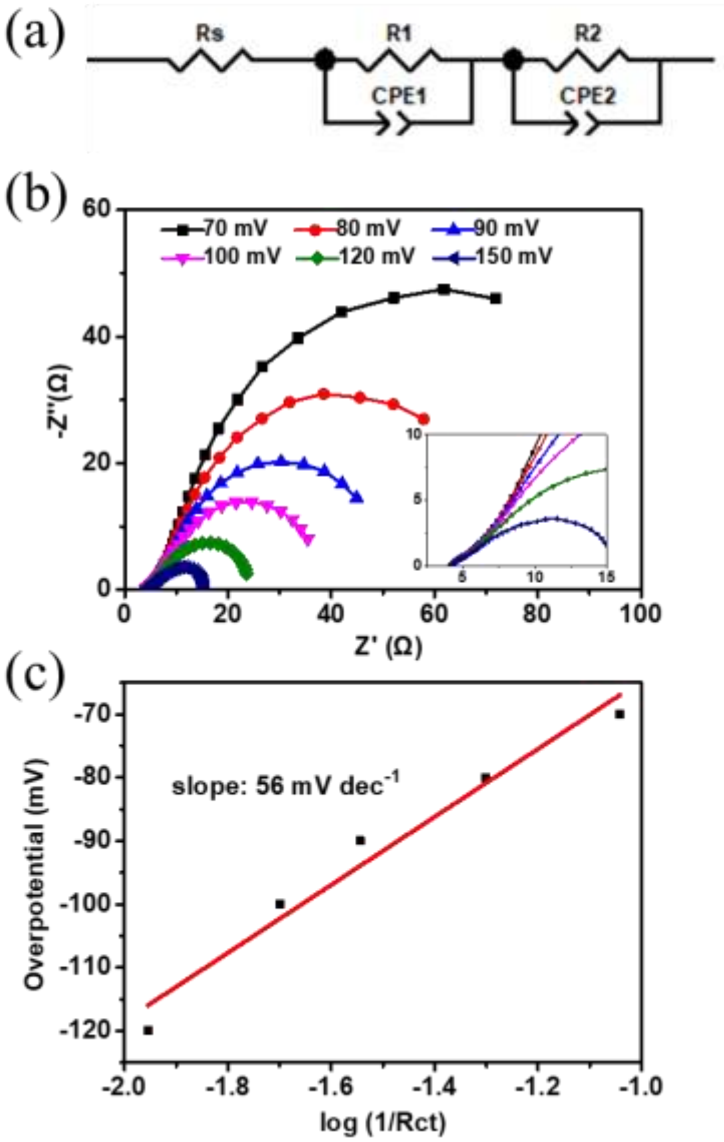

Figure S14. (a) Equivalent circuit used to model the HER process on Ni_2P@PCG at various overpotentials. (b) Nyquist plots of the impedance data of Ni_2P@PCG for HER in 0.5 M H_2SO_4. (c) The plot of overpotential *vs.* log (1/R_{ct}) and its linear fitting.

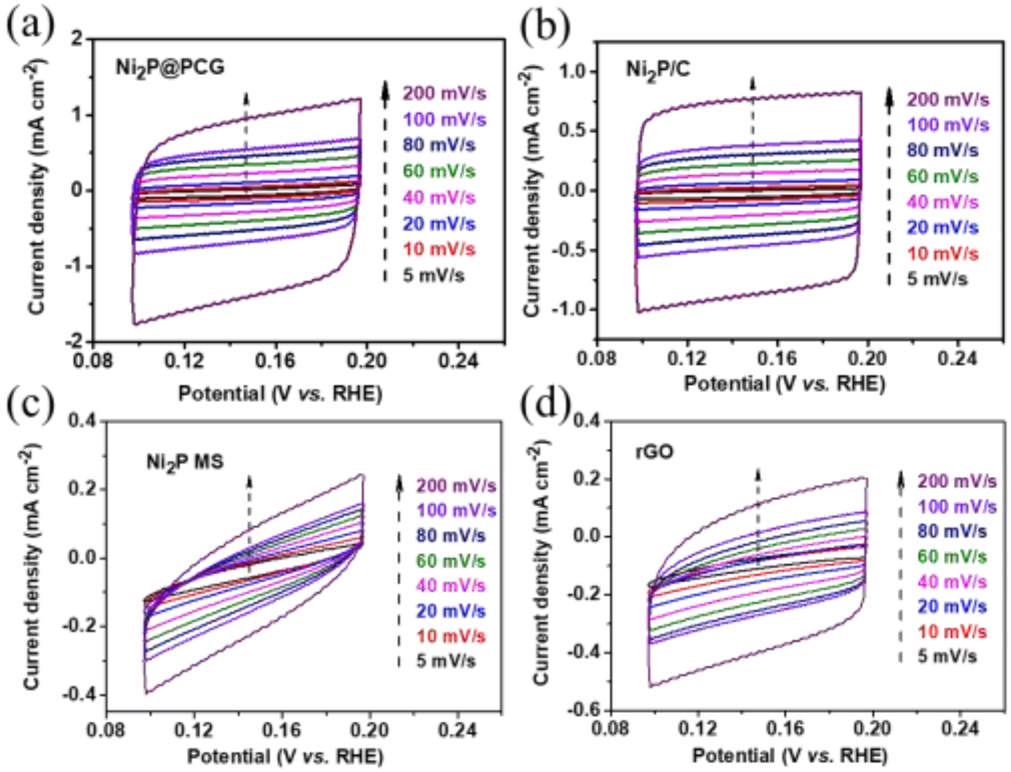

Figure S15. Non-faradaic CV scans of various electrocatalysts at 0.097~0.197 V vs RHE (-0.1~0 V vs Ag/AgCl) in 0.5 M H_2SO_4.

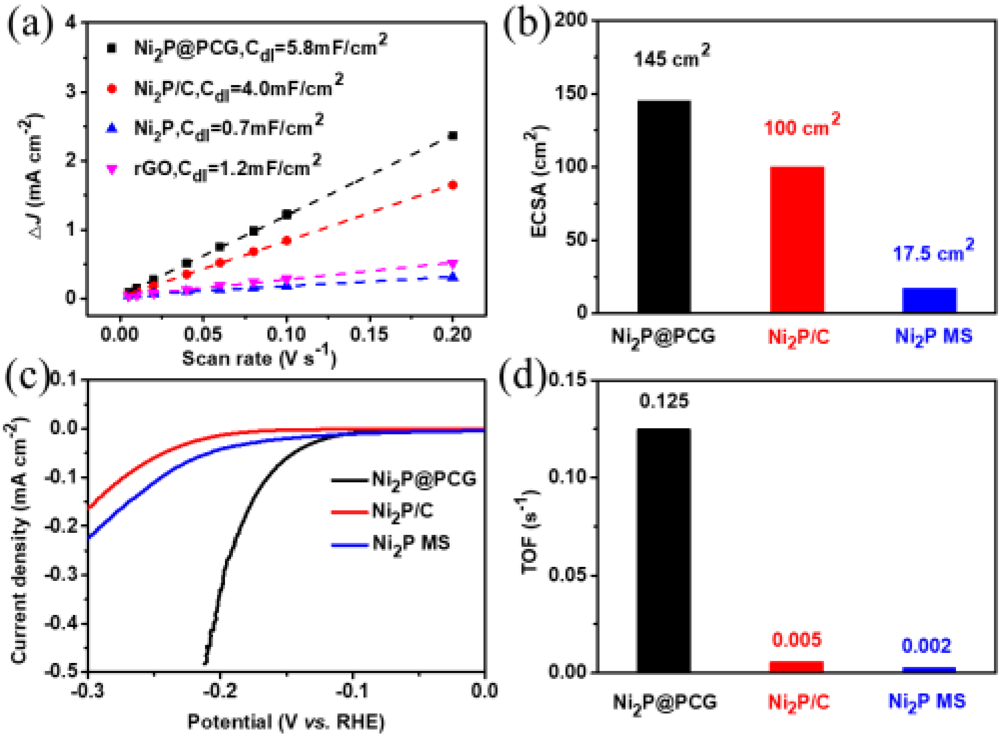

Figure S16. (a) Capacitive currents-scan rates plots of various electrocatalysts at 0.15 V *vs.* RHE. (b) The ECSA of Ni_2P@PCG, Ni_2P/C, Ni_2P MS. (c) LSV curves of the catalysts normalized by ECSAs. (d) The TOF calculated at an overpotential of -150 mV (the contents of Ni_2P in Ni_2P@PCG and Ni_2P/C were 53.7% and 35%, respectively, obtained from ICP-MS).

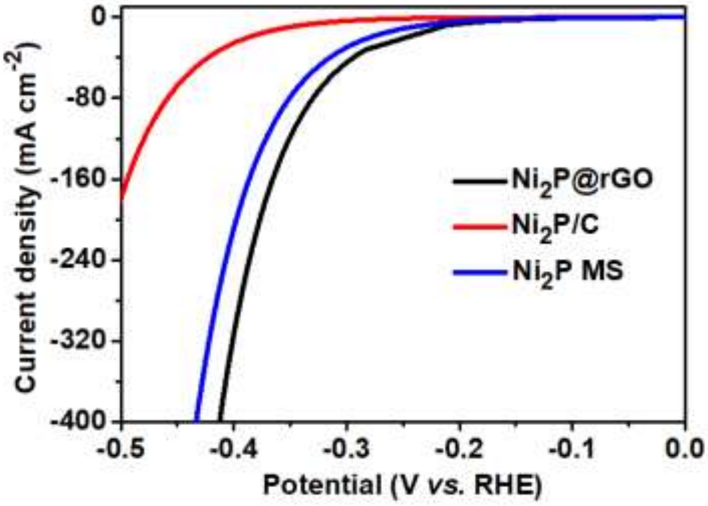

Figure S17. The LSV curves of kinetic current density for HER, fitted with simplified Butler–Volmer equation.

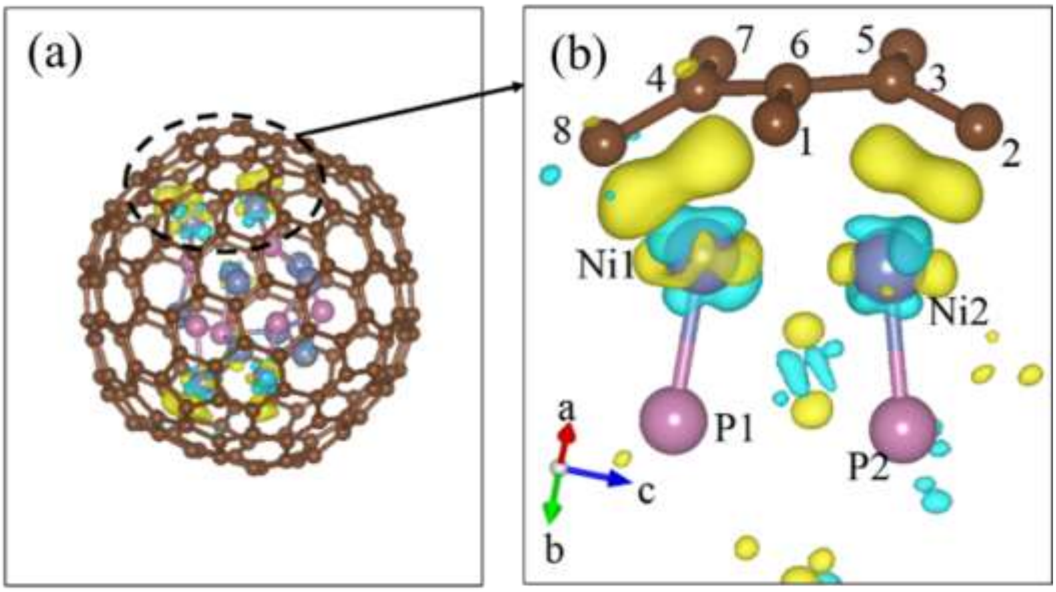

Figure S 18. (a) The original structure of Ni_2P@C. (b) Magnified diagram of differential charge density of the region in dashed black circle of (a). The yellow and cyan regions represent electron flow in and flow out. The isosurface value in (b) is 0.005 e/bohr^3. Brown: C, grey blue: Ni, grey violet: P.

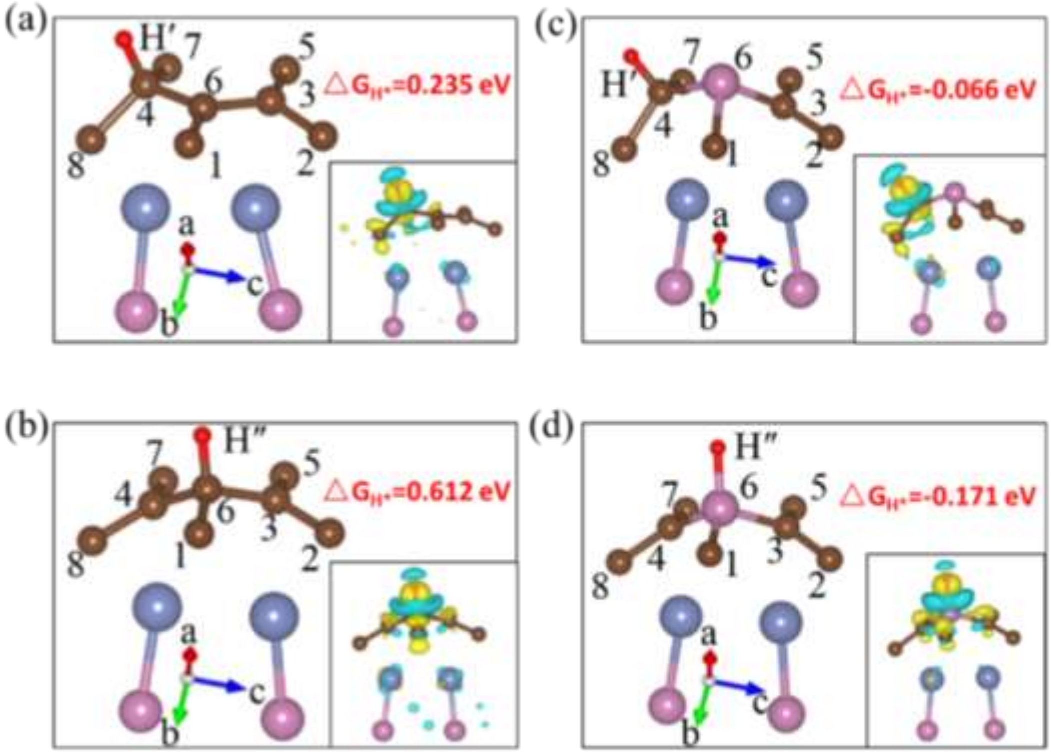

Figure S19. Theoretical models of the studied systems: The optimized structure of H adsorption and their ΔG_{H*} value. Structures of H adsorbed on 4 (H′) and 6 site (H″) of (a-b) Ni_2P@C, (c-d) Ni_2P@PC. The insert figures are the corresponding differential charge density with isosurface value of 0.005 e/bohr^3. Brown: C, grey blue: Ni, grey violet: P, red: H.

Table S1. Elemental contents of materials (atomic ratio), obtained from XPS survey.

Samples	C	O	P	Ni
Ni-P/GO	39.15	39.72	10.96	10.17
Ni_2P@PCG	67.92	20.38	6.56	5.14
Ni_2P MS	14.73	38.22	16.53	30.52
Ni_2P/C	73.36	18.55	4.13	3.96

Table S2. Comparison of typical Ni_2P based electrocatalysts for HER.

Electrocatalyst	**Mass loading (mg/cm^2)**	**Current density (mA/cm^2)**	**Overpotential (mV)**	**Exchange current density (mA/cm^2)**	**Electrolyte**	**Ref.**
Ni_2P@PCG	**0.51**	**10**	**110**	**0.13**	**0.5 M H_2SO_4**	**This work**
			150		**1.0 M KOH**	**This work**
Ni_2P /Ti	1.0	20	130	/	0.5 M H_2SO_4	*J. Am. Chem. Soc.* **2013**, *135*, 9267
			205		1.0 M KOH	
Ni_2P /Ni	-	10	128	/	0.5M H_2SO_4	*ACS Appl. Mater. Interfaces* **2016**, *8*, 12798
			183		1.0 M KOH	
Ni_2P/GCE	0.38	20	140	/	1 M H_2SO_4	*Phys. Chem. Chem. Phys.* **2014**, *16*, 5917
			250		1.0 M KOH	
Ni_2P/CNT	-	10	124	0.0537	0.5 M H_2SO_4	*J. Mater. Chem. A* **2015**, *3*, 13087
Ni_2P NPs	1.99	10	137	0.04592	0.5 M H_2SO_4	*J. Mater. Chem. A* **2015**, *3*, 1656
MOF-derived Ni_2P	0.35	10	~200	0.071	0.5 M H_2SO_4	*RSC Adv.* **2015**, *5*, 10290
CoP NCs	0.28	100	~180	/	0.5 M H_2SO_4	*Nano Lett.* **2015**, *15*, 7616.
CoP@SNC	0.61	10	174	/	1.0 M KOH	*Nanoscale* **2018**, *10*, 14613
CoNi nanoalloy	1.6	10	142	/	0.1 M H_2SO_4	*Angew. Chem.* Int. Ed. **2015**, *54*, 2100

Table S3. Atomic charge of some atoms which near the adsorbed H on site 4(H′) or site 6(H″) of the systems. The location of these sites and adsorbed H are depicted in Figure S12.

Charge / e	1	2	3	4	5	6	7	8	H
Ni_2P@C	-0.08	-0.11	-0.06	-0.08	0.04	-0.01	-0.01	-0.11	—
Ni_2P@C H′	0.04	-0.08	-0.13	-0.01	-0.01	-0.08	0.00	-0.14	0.09
Ni_2P@C H″	-0.08	-0.12	-0.06	-0.10	0.02	0.06	-0.04	-0.13	0.04
Ni_2P@PC	-0.53	-0.11	-0.54	-0.59	-0.05	1.49	-0.04	-0.06	—
Ni_2P@PC H′	-0.62	-0.14	-0.55	-0.38	-0.04	1.42	-0.07	-0.10	0.08
Ni_2P@PC H″	-0.75	-0.09	-0.77	-0.75	-0.06	2.51	-0.05	-0.12	-0.40

Table S4. The binding energy (ΔE_{H*}) and free energy of H adsorption (ΔG_{H*}) for H adsorbed on site 4 or site 6 of Ni_2P@C, Ni_2P@PC (P doped on site 6) and C_{180}.

Structure	**Site**	**ΔE_{H*} / eV**	**ΔG_{H*} / eV**
Ni_2P@C	C4	-0.005	0.235
Ni_2P@C	C6	0.372	0.612
Ni_2P@PC	**C4**	**-0.306**	**-0.066**
Ni_2P@PC	P6	-0.411	-0.171
C	C4	0.560	0.800
C	C6	0.903	1.143
Ni_2P		—	-0.54 (*J. Am. Chem. Soc.* **2013**, *135*, 9267)

References:

(1) McCrory, C. C. L.; Jung, S.; Ferrer, I. M.; Chatman, S. M.; Peters, J. C.; Jaramillo, T. F. *J. Am. Chem. Soc.* **2015**, *137*, 4347.

(2) Yan, L.; Cao, L.; Dai, P.; Gu, X.; Liu, D.; Li, L.; Wang, Y.; Zhao, X. *Adv. Funct. Mater.* **2017**, *27*, 1703455.

(3) Sun, Q.; Dong, Y.; Wang, Z.; Yin, S.; Zhao, C. *Small* **2018**, *14*, e1704137.

(4) Seh, Z. W.; Kibsgaard, J.; Dickens, C. F.; Chorkendorff, I.; Nørskov, J. K.; Jaramillo, T. F. *Science* **2017**, *355*.

(5) Dai, Z.; Geng, H.; Wang, J.; Luo, Y.; Li, B.; Zong, Y.; Yang, J.; Guo, Y.; Zheng, Y.; Wang, X.; Yan, Q. *ACS Nano* **2017**, *11*, 11031.

(6) Kresse, G.; Hafner, J. *Physical Review B* **1993**, *47*, 558.

(7) Kresse, G.; Joubert, D. *Physical Review B* **1999**, *59*, 1758.

(8) Blochl, P. E. *Physical Review B* **1994**, *50*, 17953.

(9) Hammer, B.; Hansen, L.; Norskov, J. K. *Physical Review B* **1999**, *59*, 7413.

(10) Grimme, S.; Antony, J.; Ehrlich, S.; Krieg, H. *J. Chem. Phys.* **2010**, *132*, 154104.

(11) Liu, Y.; Yu, G.; Li, G.-D.; Sun, Y.; Asefa, T.; Chen, W.; Zou, X. *Angew. Chem. Int. Ed.* **2015**, *54*, 10752.

(12) Li, J.-S.; Wang, Y.; Liu, C.-H.; Li, S.-L.; Wang, Y.-G.; Dong, L.-Z.; Dai, Z.-H.; Li, Y.-F.; Lan, Y.-Q. *Nat. Commun.* **2016**, *7*, 11204.

(13) Nørskov, J. K.; Bligaard, T.; Logadottir, A.; Kitchin, J. R.; Chen, J. G.; Pandelov, S.; Stimming, U. *Journal of The Electrochemical Society* **2005**, *152*, J23.